Front. Optoelectron. 2021, 14(3): 288–297
https://doi.org/10.1007/s12200-021-1223-3

RESEARCH ARTICLE

Ultra-thin polarization independent broadband terahertz metamaterial absorber

C. GANDHI, P. RAMESH BABU, K. SENTHILNATHAN (✉)

Department of Physics, School of Advanced Sciences, Vellore Institute of Technology, Vellore 632014, India

Abstract In this work, we present the design of a polarization independent broadband absorber in the terahertz (THz) frequency range using a metasurface resonator. The absorber comprises of three layers, of which, the top layer is made of a vanadium dioxide (VO_2) resonator with an electrical conductivity of σ = 200000 S/m; the bottom layer consists of a planar layer made of gold metal, and a dielectric layer is sandwiched between these two layers. The optimized absorber exhibits absorption greater than 90% from 2.54 – 5.54 THz. Thus, the corresponding bandwidth of the designed absorber is 3 THz. Further, the thermal tunable absorption and reflection spectra have been analyzed by varying the electrical conductivity of VO_2. The impact of the various geometrical parameters on the absorption characteristics has also been assessed. The physics of generation of broadband absorption of the proposed device has been explored using field analysis. Finally, the absorption characteristics of the unit cell has been studied for various incident and polarization angles.

Keywords terahertz (THz), metasurface, tunable absorber

1 Introduction

Recently, terahertz (THz) technology has gained a considerable attention as it can exploit the untapped slice of electromagnetic (EM) spectrum called "THz gap" which is flanked between microwave and optical regions [1,2]. While either side of this THz region has been commercialized to a larger extent by electronics and photonics, there have been many attempts to explore this virgin area too for commercialization. One of the properties of the THz region, namely, non-ionizing radiation finds potential applications in non-destructive testing, security screening and medical field [3,4]. At this juncture, we emphasize that most of the natural materials show the non-conductive and non-polar characteristics at THz frequencies and eventually result in less absorption.

It is to be noted that there are two types of classical absorbers, namely, Salisbury and Jaumann. The Salisbury absorber absorbs the incident radiation only at a particular desired frequency. On the other hand, in the Jaumann absorber, the absorption takes place at multiple resonance frequencies due to the multiple resonators and increment in the number of dielectric layers. Thus, the former one works only in the narrow band and the later one becomes bulky as it is designed with multiple resonators and several dielectric layers [5,6]. To address the above mentioned issues, metamaterial based perfect absorbers (MPAs) have been proposed. MPAs are artificial devices proposed for particular bands of the incident electromagnetic radiation and they consist of periodic structures with sub-wavelength unit cells. In general, MPAs comprise of three layers, where a dielectric layer is sandwiched between two distinct metallic layers. The absorption can be maximized by minimizing the reflection and the transmission characteristics of the proposed device. There are two key roles in designing these two distinct metallic layers. The patterned layer is used to match the surface impedance of the absorber with the surrounding air medium. This can be achieved by tailoring the constituent parameters, such as an electric permittivity and the magnetic permeability of the unit cell. As a result, reflection is minimized. The continuous metallic layer at the bottom completely blocks the transmittance of the incoming electromagnetic wave since the penetration depth of the incoming wave is greater than the thickness of the bottom layer. Hence, the absorption of the device is maximized with the minimization of both the reflectance and transmittance [7].

Received March 22, 2021; accepted June 16, 2021

E-mail: senthee@gmail.com

Topical Collection: Recent Advances in Optical Metasurfaces

MPAs were introduced in 2008 by Landy et al., and almost unity absorption in the microwave frequency regime has been reported [8]. To date, various MPAs have been designed which work in the microwave [9,10], THz [11], infrared [12] and visible [13] frequencies. Of these frequency regions, designing a perfect absorber using metamaterials (MM) in the THz frequency becomes an attractive research area. Tao et al. designed the perfect absorption in the narrow frequency range [14]. Then, dual-band [15,16], triple band [17,18], and quad-band [19,20] absorbers had been designed. These absorbers exhibited only narrow absorption bandwidth because of the resonant response of the metamaterials. Further, it is challenging to find materials with a broad absorption bandwidth and high absorption coefficients. In general, the bandwidth of the absorber is fixed once the geometrical parameters are optimized. For most of the practical applications, tunable absorption is preferred. In the THz frequency range, the following active materials, such as graphene [21–23], thermal [24–27], phase change materials [28–30], and intensity tunable materials [31,32], are used for the controllable absorption.

An ultra-broadband absorber of compact size with tunable absorption and greater efficiency is highly suitable for various applications. In this work, we design an absorber with above mentioned traits for a wide range of frequency by using a resonator made of VO_2 metasurface. The paper is written as follows. In Section 2, we present a geometrical dimension of the unit cell with material parameters. Absorption of the designed device, the associated mechanism and the material parameters are explored in Section 3. In Section 4, we have explored the physical mechanism for the generation of multiple resonances in the absorber. Further, in Section 5, we analyze the variations of the absorption spectra against the geometrical parameters of the unit cell. Finally, in Section 6, the core of the research work findings is presented.

2 Geometrical design and analysis

In this section, we describe the geometrical structure of the proposed absorber in detail. Figures 1(a) and 1(b) depict the geometrical structure of the proposed THz absorber in 3D view and front view in 2D, respectively. Here, each unit cell consists of three layers. The top layer is made of thermally tunable metasurface designed with circle and cross geometries. The metasurface is made of vanadium dioxide (VO_2) material, which varies its state from an insulator to a metal as a function of temperature. The various physical parameters of the unit cell are as follows: periodicity of the unit cell is p = 24 μm and the various dimensions of the resonators are l = 24 μm, b = 2 μm, r = 5 μm, and w = 1.5 μm. The second layer is a dielectric material made of polyimide with the dielectric permittivity of $\varepsilon = 3.5(1 + i0.002)$. The bottom layer, which is made of gold, has electrical conductivity (σ) of 5.8×10^7 S/m.

The parameters, t_1 = 0.4 μm, t_2 = 10 μm, and t_3 = 0.2 μm, represent the thicknesses of the bottom, middle and top layers, respectively. Here, the periodic boundary conditions are applied to represent a plane wave. Further, the thickness of the bottom layer is greater than the skin depth or penetration depth of the EM waves for the operating frequency range. Thus, the bottom layer prohibits the transmission of the EM waves.

At this juncture, it should be emphasized that the proposed geometrical structure can be fabricated with the existing technology. In general, the polyimide is used as a middle layer during the fabrication process. A continuous and uniform VO_2 layer can be grown by the molecular beam epitaxy method. Then the resulting layer can be patterned into a circle and cross resonator arrays using a photolithography technique. Finally, Au layer is deposited on the other side of the polyimide by electron beam lithography [33].

VO_2 acts as an insulator at room temperature and behaves as a metal beyond critical temperature (340 K).

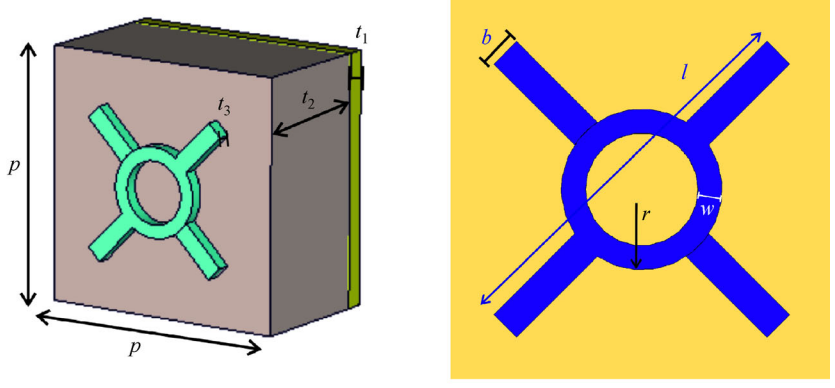

(a) (b)

Fig. 1 Geometry of the designed absorber. (a) 3D view. (b) 2D view. p = 24 μm, t_1 = 0.4 μm, t_2 = 10 μm, t_3 = 0.2 μm, l = 24 μm, b = 2 μm, r = 5 μm, and w = 1.5 μm

During the phase transition of VO_2, the lattice structure is changed from monoclinic to tetragonal state. Thus, the conductivity (σ) of VO_2 is increased from 200 to 200000 S/m. Hence, VO_2 can be used as an active material for realizing controllable optical properties. The dielectric constant of VO_2 in the THz frequency range can be represented by using the Drude model [34],

$$\varepsilon(\omega) = \varepsilon_\infty - \frac{\omega_p^2(\sigma)}{\omega^2 + i\gamma\omega}, \quad (1)$$

where the physical parameters ε_∞ (= 12) and γ (5.75×10^{13} rad/s) represent permittivity of the material at high frequency and collision frequency, respectively. Here, the frequency independent plasma frequency of VO_2 at THz frequency can be expressed as

$$\omega_p^2(\sigma) = \frac{\sigma}{\sigma_0}\omega_p^2(\sigma_0),$$

where $\sigma_0 = 3 \times 10^5$ S/m, and $\omega_p(\sigma_0) = 1.4 \times 10^{15}$ rad/s. The parameters $\omega_p^2(\sigma)$ and σ depend on the free carrier density of the electrons.

It is well known that based on the circuit model, the resonance frequency (f) is related to the inductance (L), and capacitance (C) of the resonator. Further, it can also be related to the geometrical parameters of the resonator by [35,36]

$$f = \frac{1}{2\pi\sqrt{LC}} \propto \frac{1}{l}. \quad (2)$$

Here, l represents the length of the resonator.

3 Absorption characteristics of designed unit cell

The schematic diagram shown in Fig. 2 represents the broadband absorption of designed unit cell. The maximum absorption exceeding 90% is observed from 2.54 to 5.54 THz, and the corresponding bandwidth of the absorber is 3 THz. At the resonance frequencies, the absorption reaches 100%. The relative bandwidth of the designed absorber is determined using

$$R_{BW} = 2 \times (f_u - f_l)/(f_u + f_l) \times 100\%,$$

where f_u and f_l represent the upper and lower range of frequencies with 90% of absorption efficiency [37]. The estimated relative bandwidth of the designed absorber is 74.16%.

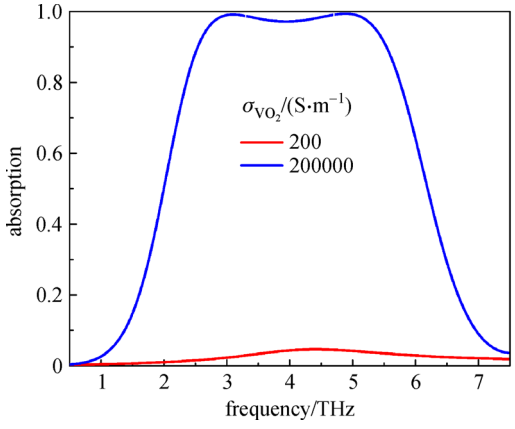

Fig. 2 Absorption of the proposed metasurface absorber in different states of the resonator

As has been discussed in the previous chapter, to understand the maximum absorption of the absorber, next, we analyze the surface impedance of the absorber in the operating frequency from 2.54 to 5.54 THz. For the metamaterials, the frequency dispersion of the effective surface impedance ($Z(\nu)$) can be described as [38]

$$Z(\nu) = \sqrt{\frac{\mu(\nu)}{\varepsilon(\nu)}} = Z' + iZ''. \quad (3)$$

Here, $\mu(\nu)$ represents the magnetic permeability, and $\varepsilon(\nu)$ describes the electric permittivity of the designed absorber. Z' and Z'' describes the real and the imaginary component of the surface impedance.

Further, the normalized form of the surface impedance in terms of the reflection (S_{11}) and transmission (S_{21}) coefficients is as follows

$$Z(\nu) = \sqrt{\frac{(1+S_{11})^2 - S_{21}^2}{(1-S_{11})^2 - S_{21}^2}}. \quad (4)$$

It is to be noted that the transmission of the absorber turns zero as the proposed unit cell possesses continuous metal plate at the bottom. Hence, the surface impedance can now be related to the reflection coefficients of the absorber as follows

$$Z(\nu) = \sqrt{\frac{1+S_{11}}{1-S_{11}}}. \quad (5)$$

The surface impedance of the absorber can be calculated by using Eq. (5). Figure 3(a) represents the real and imaginary components of the effective surface impedance of the designed absorber. From this analysis, the real part of Z_{eff} is close to unity in the frequency range from 2.54 to 5.54 THz. This clearly shows the matching of surface impedance between the top layer of the absorber with that of the surrounding air medium. As a result, the reflection turns minimum.

To understand the maximum absorption of the proposed device, now, we calculate the effective material parameters such as the effective permittivity (ε_{eff}) and effective permeability (μ_{eff}). Figure 3(b) illustrates the real and imaginary parts of ε_{eff} and μ_{eff}. From Fig. 3(b), it is observed that the real part of effective permittivity is equal to real part of effective permeability ($\varepsilon_{eff} = \mu_{eff}$) at

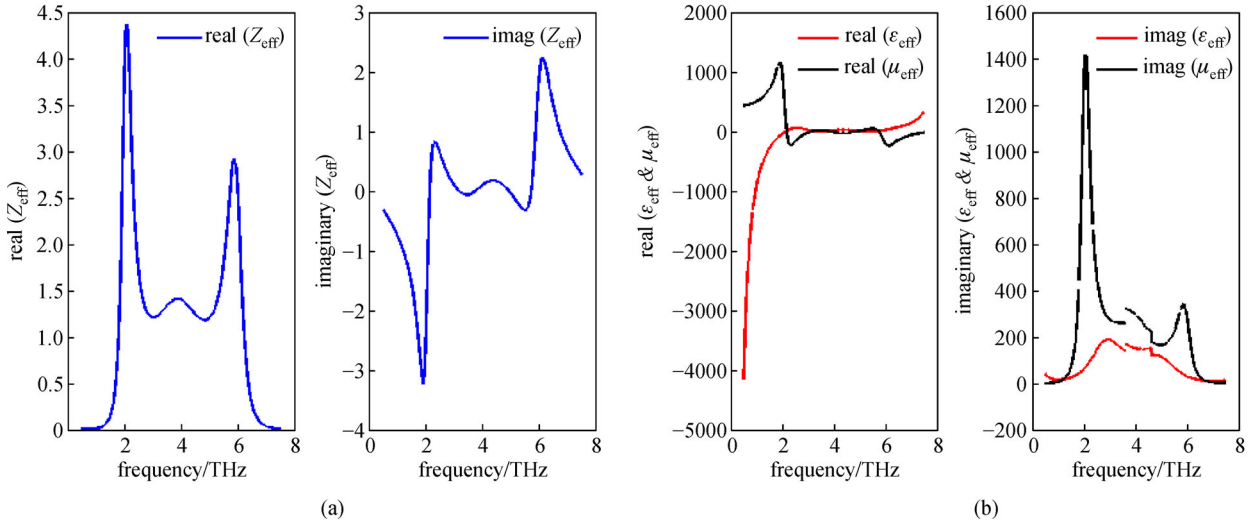

Fig. 3 Extracted material parameters. (a) Z. (b) ε-μ

resonance frequencies. As a result, the surface impedance of the proposed absorber is nearly equal to the free space. Further, the magnitude of the imaginary part of the effective material parameters turns maximum and is also equal. Thus, this ensures the maximum absorption characteristics of the absorber.

Now, we investigate the individual absorption characteristics of inner and outer resonators. In addition, we also investigate the absorption characteristics of the combined one. Figure 4(a) illustrates the absorption of the inner and the outer resonators of the unit cell. From Fig. 4(a), it is very clear that inner resonator exhibits higher absorption (50%) than the outer resonator (18%). However, we find that the absorption turns a maximum of 90% as shown in Fig. 4(b) when the outer and the inner resonators are combined.

As has been discussed in Section 2, the top layer of the resonator is made of VO_2. In this section, to understand the thermal tunable behavior of the designed absorber, we vary the electrical conductivity of the VO_2. As illustrated in Fig. 5(a), the reflection decreases as and when the electrical conductivity is increased. In other words, the corresponding absorption is increased as depicted in Fig. 5(b). We observe that absorption increases from 10% to nearly 100% when the conductivity is increased from 200 to 200000 S/m. At this juncture, we emphasize that the absorption is different for different electrical conductivity within the operating frequency. Thus, such a flexible dual-functional resonator-based absorber can be used as a perfect reflector or broadband absorber.

4 Physical mechanism

Having discussed the broadband absorption of the proposed unit cell, next, we turn to delineate the physical mechanism. Here, we analyze both the electric and the magnetic fields of the device at resonance frequencies of 3.09 and 4.89 THz. Figures 6(a), 6(b), and 6(c) represent the variations of electric field along the z-direction (E_z),

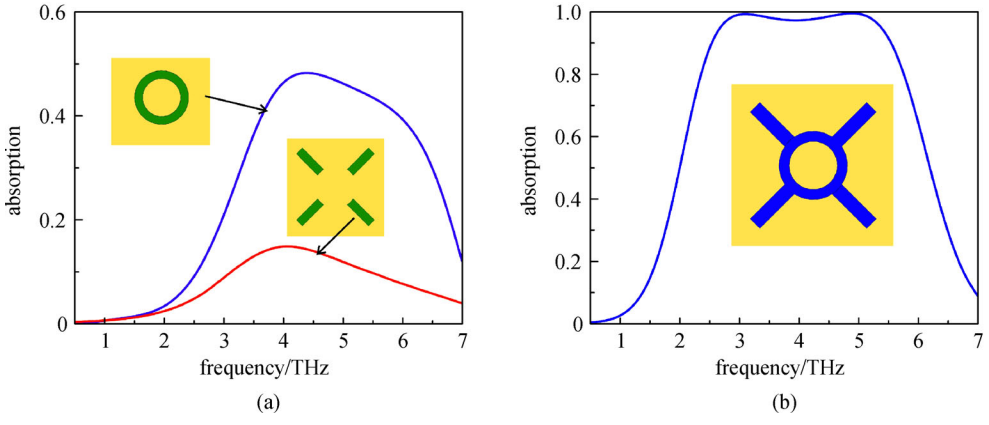

Fig. 4 Absorption. (a) Separate resonator. (b) Combination of the resonator

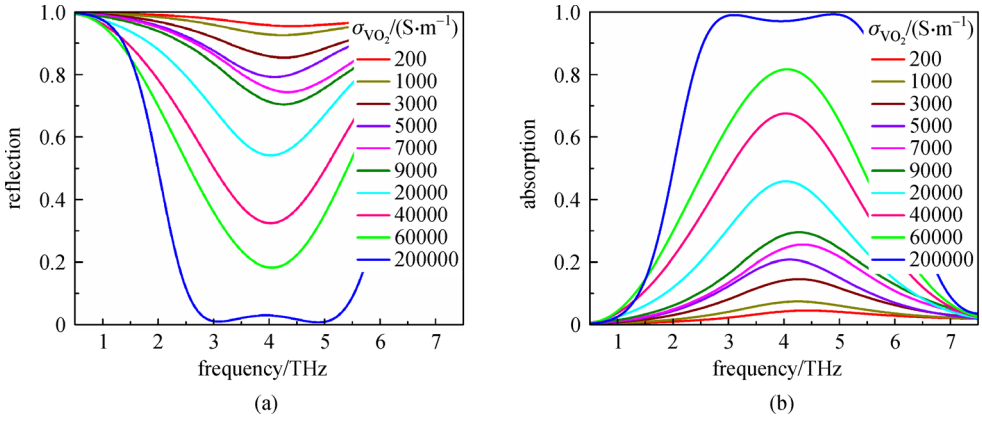

Fig. 5 Tunable reflection and absorption with electrical conductivity of VO_2. (a) Reflection. (b) Absorption

normalized electric field ($|E|$), and the magnetic field along the y-direction (H_y), respectively, at the above mentioned resonance frequencies.

Figures 6(a_1) and 6(a_2) represent the electric field distributions of E_z at 3.09 and 4.89 THz resonance frequencies, respectively. At the first resonance frequency 3.09 THz, the z-component of the electric field is distributed mainly in the cross region of the resonator and also part of the field is extended to inner resonator. This is mainly because of the resonance coupling between the inner and the outer resonators. For the second resonance frequency of 4.89 THz, the E_z field is distributed corner edges of the cross resonators.

To identify the various parts of the resonator where the charge distribution is maximum, we study the normalized electric field distributions and they are plotted in Figs. 6(b_1) and 6(b_2). From these figures, the electric field distributions of the resonator are conspicuous at the two resonance frequencies. Figures 6(c_1) and 6(c_2) represent the variation of perpendicular component of the magnetic field (H_y) at two resonance frequencies of 3.09 and 4.89 THz, respectively. The perpendicular magnetic field is distributed between the inner resonator of the metasurface and the bottom metal plate at resonance frequency of 3.09 THz. This analysis is shown in Fig. 6(c_1).

In the second resonance frequency, 4.89 THz, the distribution of the H_y component takes place between the outer resonator of the metasurface and the bottom metal plate as shown in Fig. 6(c_2). Thus, this kind of field analysis demonstrates the generation of the electric and the magnetic field distributions at the resonance frequencies.

5 Variations of absorption spectrum dependents on geometrical parameters

It is known that the EM properties of the MM are dependent on the geometrical parameters. Hence, in this section, it is of paramount importance to analyze the response of the geometrical parameters on the absorption spectra. In the parametric analysis, when one parameter of the unit cell is varied, the other parameters remain constant. To study the parametric analysis, we consider the following geometrical parameters of the absorber such as the periodicity of the unit cell (p), length of the cross shape resonator (l), width of the arm (b), radius of the circle (r), width of the circle (w), dielectric thickness (t_2), and thickness of VO_2 (t_3).

Now, we analyze the influence of length of the cross shape resonator (l) in the absorption spectra. Figure 7(a) portrays the variation of absorption spectra when the length of the cross shape resonator is varied. As shown in Fig. 7(a), increase (decrease) in length of the cross shape resonator l causes the redshift (blueshift) in the resonance frequency of the absorption spectrum. Here, the redshift (blueshift) takes place since the resonance frequency of the resonator is directly proportional to the inverse length of the resonator based on Eq. (2). As a result, the bandwidth of the absorber is increased in the former case and it is decreased in the later case.

As shown in Fig. 7(b), width of the arm affects both the absorption bandwidth and the resonance frequency. We note that the lower resonance frequency does undergo blueshift (redshift) and the higher resonance frequency undergoes redshift (blueshift) when the width of the arm is decreased (increased) from the optimized value. Thus, the bandwidth of the absorber decreases (increases) when width of the arm is decreased (increased) from the optimized value.

From Fig. 7(c), it is very clear that the radius of the circle does not affect the absorption spectra as the variations are very tiny. However, there is appreciable change in absorption spectra when the width of the circle is varied. As depicted in Fig. 7(d), the bandwidth increases (decreases) when the width of the circle is decreased (increased).

As shown in Fig. 7(e), we find that the absorption bandwidth and the resonance frequency of the designed absorber are changed with the periodicity of the unit cell. As a result, the bandwidth increases (decreases) when the

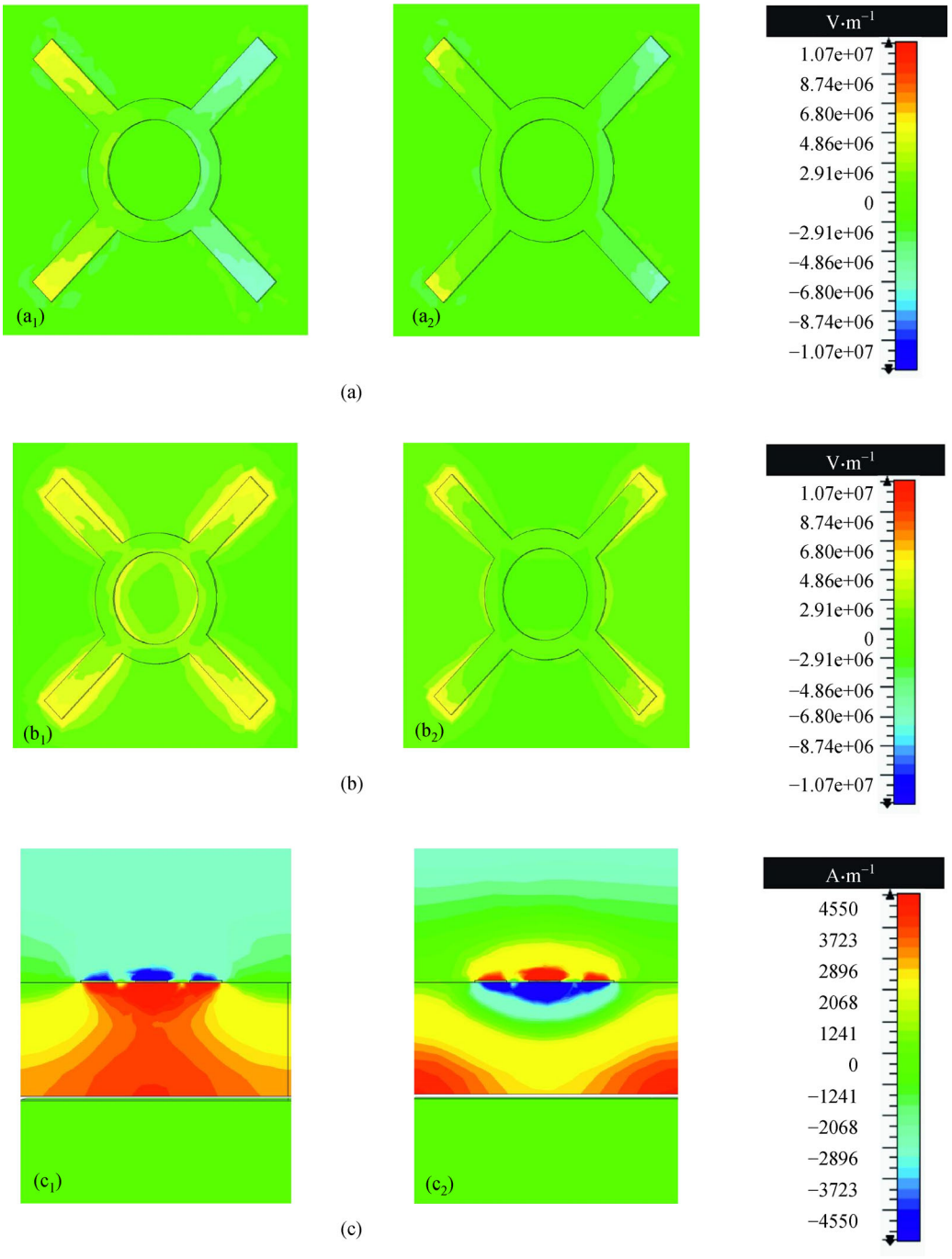

Fig. 6 Field distribution at resonance frequencies of 3.09 and 4.89 THz. (a) Electric field along the *z*-direction. (b) Normalized electric field. (c) Magnetic field along the *y*-direction

periodicity of the unit cell is decreased (increased) from the optimized value. This is because of the resonance coupling between the resonators of the unit cell.

So far, we have discussed the impact of length and width of the unit cell against absorption spectra. In the last part of the parametric analysis, we delineate the influence of the thickness of VO_2 as well as thickness of dielectric layer over the absorption spectra. Here, we vary the thickness of VO_2 by keeping the electrical conductivity as 200000 S/m. Figures 8(a) and 8(b) show the variations of the absorption against the thickness of the metasurface VO_2 resonator and the dielectric layer, respectively. From Fig. 8(a), the absorption decreases (increases) when the thickness of VO_2 is increased (decreased) from the optimized value. From Fig. 8(b), we observe that both the lower and higher resonance frequencies undergo blueshift when the

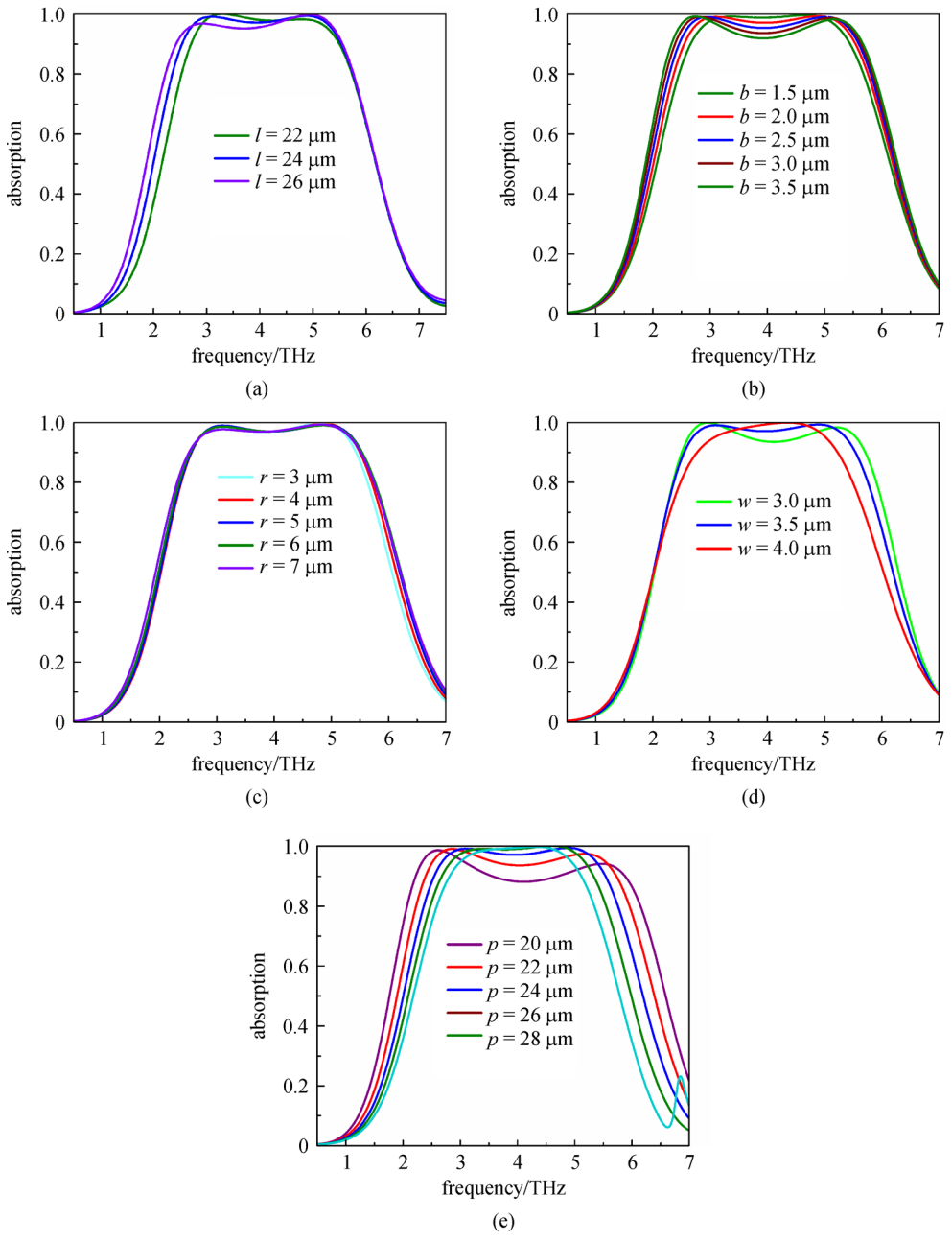

Fig. 7 Analysis of absorption over various geometrical parameters. (a) Length of the strip. (b) Width of the strip. (c) Outer radius of the circle. (d) Width of the circle. (e) Periodicity of the unit cell

dielectric thickness is decreased. As a result, there is an increment in the bandwidth and decrement in the efficiency. We find that both bandwidth and efficiency decrease when the dielectric thickness is increased from the optimized value. The reason for this shift is due to the changes in the effective cavity length of the absorber. Further, increase in dielectric thickness affects the interaction between the bottom metal plate and the top metal resonator. These parametric studies corroborate that the absorption spectra are robust against variations in most of the geometrical parameters.

To understand the performance of the absorber, we analyze the absorption responses for the various oblique incidences other than the normal incidence angle. Here, the incident EM waves make an angle θ with the unit cell of the absorber. Further, the absorption characteristics are examined for various incident angles of transverse electric (TE) and transverse magnetic (TM) polarizations. Figures 9(a) and 9(b) describe the absorption response of the absorber for various incident angles (θ) from 0° to 80°. From the analysis, the absorber exceeds the absorption efficiency of 90% up to 40° of the incident angles. Because

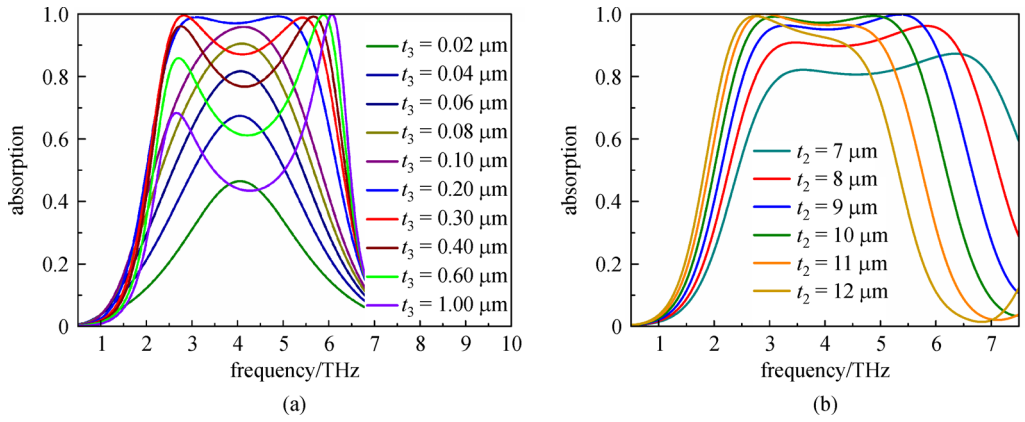

Fig. 8 Thickness response of (a) top resonator VO_2 (t_3) and (b) dielectric layer (t_2)

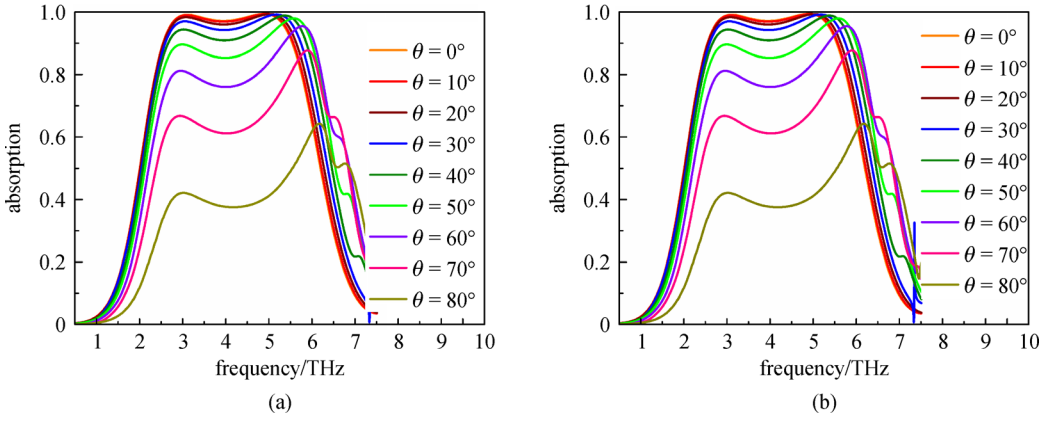

Fig. 9 Incident angle sensitivity of the absorber. (a) TE mode of polarization. (b) TM mode of polarization

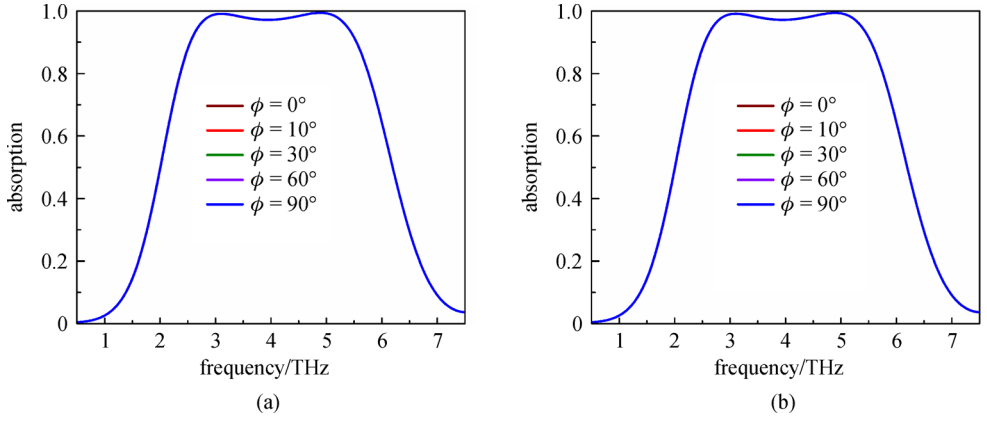

Fig. 10 Absorption of proposed absorber for different polarization angle. (a) TE polarization. (b) TM polarization

of the symmetry of the geometry, the absorption response is the same for the TM polarization. Here, the maximum absorption is maintained up to 40°.

Next, we analyze the absorption characteristics for the various polarization angles. Figures 10(a) and 10(b) illustrate the absorption of the unit cell for different polarization angles. From this analysis, we find that the absorption characteristics remain same for various polarization angles. Because of the geometrical symmetry of the absorber, the absorption exhibits the same responses for both the TE and TM polarizations. Thus, the proposed unit cell is polarization insensitive.

6 Conclusions

In conclusion, we have designed a three layer metamaterial absorber that absorbs the incoming radiation for a wide range of frequencies. The proposed absorber exhibits a maximum absorption exceeding 90% from 2.54 to 5.54 THz when the conductivity is 200000 S/m. Thus, the bandwidth of the absorber is 3 THz. Then, we have discussed the physical mechanism of the proposed absorber with the help of field analysis. Further, in order to study the robustness of the proposed absorber, we have carried out the influence of the various geometrical parameters over the absorption spectra. These numerical results encourage that the proposed absorber is a robust one against the variations in the various geometrical parameters of the unit cell. Finally, we have also studied the sensitivity for various incident and polarization angles. It has been found that the absorber maintains 90% efficiency up to 40° incident angles and it is also polarization insensitive. Based on the above results, we are of the opinion that the designed THz metasurface absorber would turn out to be a potential candidate in communication, radar and stealth technology.

References

1. Sirtori C. Bridge for the terahertz gap. Nature, 2002, 417(6885): 132–133
2. Tonouchi M. Cutting-edge terahertz technology. Nature Photonics, 2007, 1(2): 97–105
3. Jepsen P U, Cooke D G, Koch M. Terahertz spectroscopy and imaging–modern techniques and applications. Laser & Photonics Reviews, 2011, 5(1): 124–166
4. Federici J F, Schulkin B, Huang F, Gary D, Barat R, Oliveira F, Zimdars D. THz imaging and sensing for security applications—explosives, weapons and drugs. Semiconductor Science and Technology, 2005, 20(7): S266–S280
5. Salisbury W W. Absorbent body for electromagnetic waves. United States Patent US 2599944. 1952
6. Knott E F, Schaeffer J F, Tulley M T. Radar Cross Section. Raleigh: SciTech Publishing, 2004
7. Watts C M, Liu X, Padilla W J. Metamaterial electromagnetic wave absorbers. Advanced Materials, 2012, 24(23): OP98–OP120, OP181
8. Landy N I, Sajuyigbe S, Mock J J, Smith D R, Padilla W J. Perfect metamaterial absorber. Physical Review Letters, 2008, 100(20): 207402
9. Li H, Yuan L H, Zhou B, Shen X P, Cheng Q, Cui T J. Ultrathin multiband gigahertz metamaterial absorbers. Journal of Applied Physics, 2011, 110(1): 014909
10. Sharma S K, Ghosh S, Srivastava K V. An ultra-thin triple-band polarization-insensitive metamaterial absorber for S, C and X band applications. Applied Physics A, Materials Science & Processing, 2016, 122(12): 1071
11. Wen Y, Ma W, Bailey J, Matmon G, Yu X. Broadband terahertz metamaterial absorber based on asymmetric resonators with perfect absorption. IEEE Transactions on Terahertz Science and Technology, 2015, 5(3): 406–411
12. Zhang B, Zhao Y, Hao Q, Kiraly B, Khoo I C, Chen S, Huang T J. Polarization-independent dual-band infrared perfect absorber based on a metal-dielectric-metal elliptical nanodisk array. Optics Express, 2011, 19(16): 15221–15228
13. Ghobadi A, Dereshgi S A, Hajian H, Bozok B, Butun B, Ozbay E. Ultra-broadband, wide angle absorber utilizing metal insulator multilayers stack with a multi-thickness metal surface texture. Scientific Reports, 2017, 7(1): 4755
14. Tao H, Landy N I, Bingham C M, Zhang X, Averitt R D, Padilla W J. A metamaterial absorber for the terahertz regime: design, fabrication and characterization. Optics Express, 2008, 16(10): 7181–7188
15. Wang B X, Xie Q, Dong G, Huang W Q. Broadband terahertz perfect light absorber based on the modes of fundamental response and surface lattice resonance. OSA Continuum, 2018, 1(1): 213–220
16. Wen Q Y, Zhang H W, Xie Y S, Yang Q H, Liu Y L. Dual band terahertz metamaterial absorber: design, fabrication, and characterization. Applied Physics Letters, 2009, 95(24): 241111
17. Chen C, Can S, Schalch J, Zhao X, Duan G, Averitt R D, Zhang X. Ultrathin terahertz triple-band metamaterial absorbers: consideration of interlayer coupling. Physical Review Applied, 2020, 14(5): 054021
18. Wang B X, Tang C, Niu Q, He Y, Chen T. Design of narrow discrete distances of dual-/triple-band terahertz metamaterial absorbers. Nanoscale Research Letters, 2019, 14(1): 64
19. Liu S, Zhuge J, Ma S, Chen H, Bao D, He Q, Zhou L, Cui T J. A bi-layered quad-band metamaterial absorber at terahertz frequencies. Journal of Applied Physics, 2015, 118(24): 245304
20. Wang B X, Wang G Z. Quad-band terahertz absorber based on a simple design of metamaterial resonator. IEEE Photonics Journal, 2016, 8(6): 1–8
21. Arabmohammadi M, Kashani Z G, Sheikhan R A. Numerical analysis and circuit model of tunable dual-band terahertz absorbers composed of concentric graphene disks and rings. Journal of Electronic Materials, 2020, 49(10): 5721–5729
22. Su W, Chen X, Geng Z. Dynamically tunable dual-frequency terahertz absorber based on graphene rings. IEEE Photonics Journal, 2019, 11(6): 1–8
23. Nejat M, Nozhat N. Design, theory, and circuit model of wideband, tunable and polarization-insensitive terahertz absorber based on graphene. IEEE Transactions on Nanotechnology, 2019, 18: 684–690
24. Huang X, He W, Yang F, Ran J, Yang Q, Xie S. Thermally tunable metamaterial absorber based on strontium titanate in the terahertz regime. Optical Materials Express, 2019, 9(3): 1377–1385
25. Wang Z L, Hu C X, Liu H B, Zhang H F. A newfangled terahertz absorber tuned temper by temperature field doped by the liquid metal. Plasmonics, 2021, 16(2): 425–434
26. Zhang H F, Wang Z L, Hu C X, Liu H B. A tailored broadband terahertz metamaterial absorber based on the thermal expansion feature of liquid metal. Results in Physics, 2020, 16: 102937
27. Luo H, Cheng Y. Thermally tunable terahertz metasurface absorber

based on all dielectric indium antimonide resonator structure. Optical Materials, 2020, 102: 109801
28. Kong X R, Dao R N, Zhang H F. A tunable double-decker ultra-broadband THz absorber based on a phase change material. Plasmonics, 2019, 14(5): 1233–1241
29. Zhang Y, Wu P, Zhou Z, Chen X, Yi Z, Zhu J, Zhang T, Jile H. Study on temperature adjustable terahertz metamaterial absorber based on vanadium dioxide. IEEE Access: Practical Innovations, Open Solutions, 2020, 8: 85154–85161
30. Zhang C, Huang C, Pu M, Song J, Luo X. Tunable absorbers based on an electrically controlled resistive layer. Plasmonics, 2019, 14(2): 327–333
31. Yuan S, Yang R, Tian J, Zhang W. A photoexcited switchable tristate terahertz metamaterial absorber. International Journal of RF and Microwave Computer-Aided Engineering, 2020, 30(1): e22014
32. Wang B X, Wang G Z, Zhu H. Quad-band terahertz absorption enabled using a rectangle-shaped resonator cut with an air gap. RSC Advances, 2017, 7(43): 26888–26893
33. Cai H, Chen S, Zou C, Huang Q, Liu Y, Hu X, Fu Z, Zhao Y, He H, Lu Y. Multifunctional hybrid metasurfaces for dynamic tuning of terahertz waves. Advanced Optical Materials, 2018, 6(14): 1800257
34. Wang S, Kang L, Werner D H. Hybrid resonators and highly tunable terahertz metamaterials enabled by vanadium dioxide (VO_2). Scientific Reports, 2017, 7(1): 4326
35. Zhou J, Zhang L, Tuttle G, Koschny T, Soukoulis C M. Negative index materials using simple short wire pairs. Physical Review B, 2006, 73(4): 041101
36. Ye Y Q, Jin Y, He S. Omnidirectional, polarization-insensitive and broadband thin absorber in the terahertz regime. Journal of the Optical Society of America B, Optical Physics, 2010, 27(3): 498–504
37. Ding F, Cui Y, Ge X, Jin Y, He S. Ultra-broadband microwave metamaterial absorber. Applied Physics Letters, 2012, 100(10): 103506
38. Smith D R, Vier D C, Koschny T, Soukoulis C M. Electromagnetic parameter retrieval from inhomogeneous metamaterials. Physical Review E, 2005, 71(3 Pt 2B): 036617

C. Gandhi received his M.Sc. degree in Physics from Loyola College, India. He received his Ph.D. degree in Physics from Vellore Institute of Technology, India. His main research interests include terahertz absorber and polarization converter using metamaterials.

P. Ramesh Babu has worked in the Department of Physics at Vellore Institute of Technology, India, for the last thirty years, of which, he has been a professor since 2009. He received his Ph.D. degree from University of Madras, India, in 2006. His doctoral thesis focussed on the generation of Bragg solitons in a photonic bandgap structure. His research interests include nonlinear fiber optics, photonic crystal fibers, Bose–Einstein condensation, metamaterials and plasmonic sensors. He has published more than 50 papers in high-profile journals that include *IEEE Journal of Selected Topics in Quantum Electronics*, *IEEE Sensors*, *Optical Fiber Technology*, *Current Science*, *Journal of Modern Optics*, *Optical Engineering*, etc. He is a life member of Indian Association of Physics Teachers, Indian Laser Association and Indian Society for Technical Education.

K. Senthilnathan is a professor at Vellore Institute of Technology (VIT), India. He earned his M.Sc. and M.Phil. degrees in Physics from the University of Madras, India, and Ph.D. degree from Anna University, India. He carried out post-doctoral research at The Hong Kong Polytechnic University, China, from Dec. 2005 to Aug. 2008. Then, he served as Assistant Professor in NIT Rourkela from Sep. 2008 to Jun. 2010. Later, he joined VIT in Jul. 2010 as Assistant Professor. His areas of research include optical fibers, fiber Bragg gratings, photonic crystal fibers, pulse compression, Bose–Einstein condensation and metamaterials. Besides, he has also been focusing on developing various types of fiber sensors including micro-structured fibers. These results have been disseminated in various prestigious international journals that include *Journal of the Optical Society of America B*, *IEEE Journal of Quantum Electronics*, *IEEE Journal of Lightwave Technology*, *IEEE Photonics Technology Letters*, *IEEE Sensors*, *IEEE Journal of Selected Topics in Quantum Electronics*, etc. He has more than 100 Scopus indexed publications.